Journal of Materials Science and Engineering A 3 (8) (2013) 531-539

Microstructural Study of the Intermetallic Bonding Between Al Foam and Low Carbon Steel

Michele Monno[1, 2], Valerio Mussi[1], Daniela Negri[1], Luca Zampori[3] and Giovanni Dotelli[3]

1 Machine Tools and Production Systems Laboratory, MUSP Laboratory, Piacenza 29122, Italy

2 Mechanical Engineering Department, Politecnico di Milano, Milano 20156, Italy

3 Department of Chemistry, Materials and Chemical Engineering, "G. Natta", Politecnico di Milano, Milano 20133, Italy

Received: May 23, 2013 / Accepted: July 06, 2013 / Published: August 10, 2013.

Abstract: Bonding between a metal foam core and a metallic skin is a pre requisite for the technological application of aluminum foam as filling reinforcement material to improve energy absorption and vibration damping of hollow components. This work is a preliminary study for the microstructural characterization of the interface layer formed between a commercial powder metallurgy (PM) precursor and a steel mould during foaming. The microstructure of the intermetallic layer was characterized by scanning electron microscopy, electron probe microanalysis and nanohardness measurements on the cross section. X-ray diffraction measurements, performed on the foam/substrate surface after stepwise material removal, allow the identification of the intermetallic phases. Two intermetallic layers, identified as Fe_2Al_5 and $FeAl_3$, characterize the low Si foam/substrate while the AlSi10 foam/substrate interface evidences the presence of three Fe(Si, Al) intermetallic layers with different composition. Two and three different phases of increasing hardness could be distinguished going from the foam to the steel substrate for AlMg1Si0.6 and AlSi10 precursors respectively. The results suggest the importance of elemental diffusion from steel substrate in the molten aluminum matrix (foam). The possibility to control and tailor the microstructural properties of the interface between foam and steel skin is of fundamental importance in the technological process of foam filled structures manufacturing.

Key words: Metal foam, intermetallic layer, phase identification.

1. Introduction

Metal foams are promising materials in applications where lightness and high stiffness combined with acceptable manufacturing costs are of prime interest. Due to their cellular structure they have high energy absorption and damping capacities. As a consequence light aluminium metal foams have been proposed as filling reinforcement of hollow structures for example to improve impact behaviour in protection systems in automotive field or as vibration dampers in machine tools. When metal foams are used to improve stiffness the achieving of high performance (higher bending and torsional stiffness of the reinforced structure than those of the starting component) requires a good bonding between the hollow structure and the filling foam. A continuous metallurgical bond constituted by an intermetallic layer seems to guarantee the sealing and to ensure a perfect mechanical connection.

Many researchers [1-3] suggest the technological importance of a metallurgical connection between metal foam and metallic skin but the process of formation of the interlayer and the correlation between the phases formed and the mechanical proprieties has not been clarified up to now. The formation of the metallurgical bonding seems to be hampered by the short contact time between the solid metal and the molten aluminium during the foaming process and by the oxidation of both the foam and the internal mould surface during the expansion. Recent results [1, 4, 5] suggest that foaming process performed in inert atmosphere favours the formation of a continuous intermetallic layer between foam and substrate.

Corresponding author: Daniela Negri, Ph.D., research field: metal foams. E-mail: daniela.negri@musp.it.

The formation of an intermetallic layer when solid iron comes in contact with molten aluminium is typical of several technological processes (joining, hot dip aluminizing, permanent mould casting, high pressure die casting, manufacturing of bimetallic parts, etc.). Diffusion of Fe and Al atoms leads to the formation and growth of the intermetallic layer through a process that initially is reaction diffusion and then follows parabolic kinetics during its growth [6-10]. The Fe_2Al_5 and $FeAl_3$ phases have been identified as the phases formed in the temperature range around 700 °C (suitable for Al metal foaming). Microstructural studies suggest the Fe_2Al_5 as the major constituent phase of the intermetallic layer instead of $FeAl_3$. The properties of the intermetallic layer seem to depend on the type, morphology and thickness of the phases formed. Many research works studied the effects of different alloying elements in the composition of the steel and aluminium melt (C, Si, Fe, Mn, Ti and Ni) [11-15] on the thickness and morphology of the intermetallic layers to improve tensile strength, elongation and ductility, neutralising the brittleness of AlFe and AlFeSi intermetallics for aluminium melt in contact with solid metal.

The formation and growth rate of the different intermetallics depend on their interdiffusion coefficients [16] that is phases with higher diffusivity grow faster. The intermetallic layer at Al and Al-Si foam/low carbon steel interface predominantly consists of aluminium, iron and silicon atoms. Therefore, as suggested for low C steel: Al joining [15], it is of fundamental and technological importance to understand how these elements distribute, to which kind of phase they give rise and their nucleation and growth kinetics but it is not the main purpose of this work.

This work aims at describing in detail the microstructure of the intermetallic layer formed at the interface between an Al foam, starting from commercial powder metallurgy (PM) precursors of different compositions, and a low carbon steel plate during foaming in inert atmosphere (Ar flow). The foam expansion was constrained by a closed mould. A qualitative and semi quantitative investigation allowed to identify the various phases present at different depth in the intermetallic layer. Suitable and well stated experimental conditions have been used in this work ($T_{furnace}$ = 700 °C, $t_{in\ the\ furnace}$ = 10 min). Further analysis considering different process parameters (temperature, time, atmosphere and cooling conditions) is in progress to understand if and how their changes influence the morphology and mechanical properties of the intermetallic layer.

2. Experiments

The formation of metallurgical bonding between foam, prepared by powder metallurgical (PM) route, and a solid metal substrate was investigated. Precursors of two different compositions were foamed on a S355J2 low carbon steel (0.188 wt% C) plate:

AlSi10 which contains 0.8 wt% TiH_2 as blowing agent and is very close to the eutectic composition;

AlMg1Si0.6 (0.8 wt% TiH_2), chosen in order to reduce the potentially negative effect of silicon in wetting between Al and Fe.

Specimens were cut from cylindrical commercial precursors. They were mechanically polished with emery papers to obtain a smooth contact with the steel substrate and therefore a uniform heat transfer during heating. The steel substrates were prepared by cutting and grinding tablets of diameter 56 mm and thickness 4.5 mm. Precursor pieces on the steel substrates were arranged in the equipment sketched in Fig. 1 and foamed in argon flow for 10 min in a convection furnace pre heated at 700 °C. The thermal history of the specimens was followed by means of two thermocouples (K type): one directly into the specimen and the second positioned under the sample holder (see the schematic drawing in Fig. 1).

The foamed specimens (substrate and foam) were cut perpendicular to the substrate surface using a

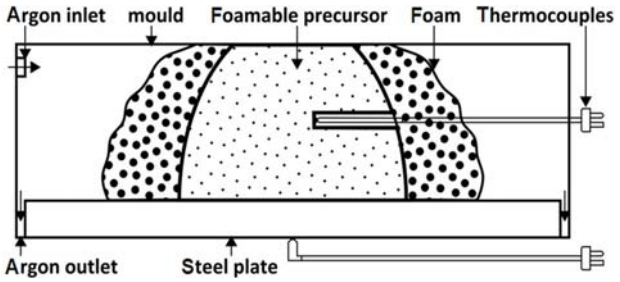

Fig. 1 Schematic draw of the equipment used for foaming.

diamond blade and prepared for microstructural examination of the interface. The as prepared cross sections were observed by electron microscopy. The specimens surfaces were sputter coated with gold to prevent electron charge up during SEM observation. ZEIS EVO 50 XVP scanning electron microscope (resolution: 3 nm for secondary electron and 4.5 nm for back scattered electron) coupled with an INCA Energy 200 dispersive X-ray (EDS) system was used to distinguish the different phases present in the layer and to propose a phase identification through its elemental composition. Thickness of the intermetallic layers was determined using a plug-in project by Sacha [17] in ImageJ software for image analysis [18] using a seeded region growing technique [19, 20] measuring the area of each layer and dividing it by its width.

To perform a qualitative and semi quantitative investigation of the intermetallic layer, a detailed study of the specimens surface was performed at various depth. Foam was polished out by steps of around 20-30 μm until the intermetallic layer was reached then thinner thicknesses of material was removed in order to penetrate deeply in the layer. At each grinding step the specimen surfaces were observed by XRD and energy dispersive X-ray analysis (EDX). Diffractograms were collected using Cu-K_α radiation in the range of $5° \leq 2\theta \leq 70°$ with a step size of 0.02^o and a counting time of 4 s per step with a Brucker D8 Advance diffractometer. X-ray diffraction measurements allowed phase identification. Nano hardness measurements were performed across the interface of the intermetallic layer to obtain information about the hardness of the phases detected. A Hardness Tester CSM Instruments equipped with a triangular pyramid-shaped diamond with an edge angle of $\theta = 115$ °C (Berkovich indenter) was used. This indenter is characterised by the same projected area/penetration depth ratio of a Vickers indenter (this way the two measurements are comparable). The Oliver and Pharr method [21] allowed to extract nano hardness and elastic modulus from unloading part of the force-displacement curve. Indentations have been arranged by setting a penetration depth of 200 nm. Indentations were then observed by backscattered electrons in order to identify the belonging layer of each spot.

3. Experimental Results

3.1 Foaming Conditions

Preliminary tests showed that constraining the foam expansion improves the formation of metallurgical bonding: it prevents the argon or air to stir up the sample in the first instants when the foam expands upwards maximizing the contact (both time and surface) between foam and solid substrate. In subsequent experiments, precursors have been foamed partially constrained using the equipment sketched in Fig. 1; the mould provides both a chamber for gas protection and a boundary against upward expansion of the foam. Argon flows from two lateral holes in order to uniformly wrap the precursor tablet. Precursors, while foaming, stand on ground substrate which provides both a flat surface that allows the progressive removal of material parallel to the bottom face and fine notches that could favour the adhesion process. The thermocouple inserted in the precursor billet allowed to record the temperature evolution during the foaming process. The temperature vs. time curves are plotted in Fig. 2. The small changes in the curvature of the heating curve at temperature around 578 °C and 655 °C are representative of the melting interval of AlSi10 and AlMg1Si0.6 precursors respectively while those on the cooling curve underline the solidification of the foamed samples. Cooling is slower as it is performed in air outside the furnace.

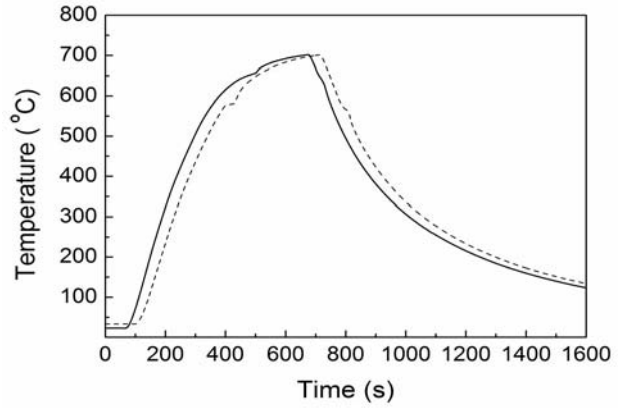

Fig. 2 Temperature evolution of AlSi10 (dashed line) and AlMg1Si0.6 (solid line) precursors during foaming on the low carbon steel plate.

3.2 Microstructure Characterization of Specimens' Cross Section

At foaming temperature (T = 700 °C) the liquid foam comes in contact with solid steel. Similarly to what reported in literature for dipping experiments of solid iron in molten aluminium, during foaming, iron atoms can easily diffuse from the substrate into molten foam and aluminium atoms diffuse towards the substrate with a lower rate. An intermetallic layer forms and further growth depends on the diffusion of Fe atoms towards foam and of Al atoms to the substrate within the intermetallic layer. Therefore, since easier diffusion of aluminium is expected [22] the intermetallic phase seems to grow towards the iron rich substrate. This chemical reaction can occur only if the liquid aluminium wets the solid substrate. A continuous intermetallic layer forms between foam and substrate when liquid foam of both compositions comes in contact with solid steel substrate during foaming in argon flux. Backscattered electron images by scanning electron microscopy (SEM) (Fig. 3) of the interface allow to clearly recognise the aluminium foam (dark grey), the iron substrate (bright grey) and the intermetallic layer between them. It is possible to observe a continuum and uniform bonding layer between foam and substrate for both compositions. As it can be assumed that any intermetallic phase, generated during the foaming process, is the result of the contact between the liquid foam and the solid steel, it is reasonable to observe dependence from the precursor composition in the formation of the layer. A quite continuum layer develops both for AlMg1Si0.6 and AlSi10. A 40 μm layer is observed for the first composition while a thinner thickness of around 24 μm characterises the precursor containing more Si (Fig. 3b) [23] which hampers wetting between Al and Fe and retards the formation and growth of intermetallics [24].

Backscattered SEM images at higher magnification, reported in Fig. 4, clearly show the formation of a two phase layer for AlMg1Si0.6 precursor, while a threefold layer is observed for AlSi10 precursor. The average elemental percentages, detected by electron

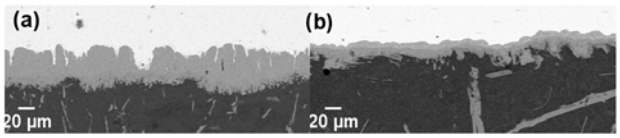

Fig. 3 Scanning electron micrographs (BSE signal) of the interface between foam and steel substrate: (a) AlMg1Si0.6 and (b) AlSi10.

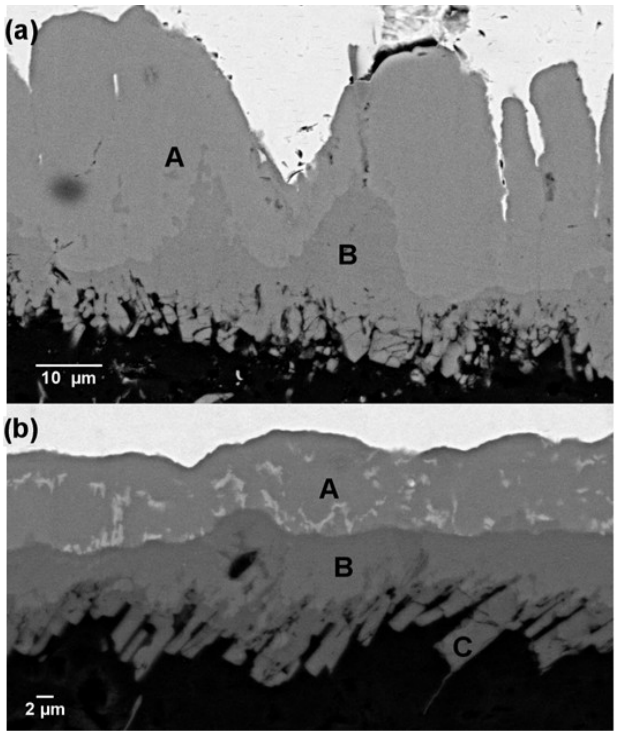

Fig. 4 Scanning electron micrographs (BSE signal) of the interface between foam and steel substrate: (a) AlMg1Si0.6 foamed in argon and (b) AlSi10 foamed in argon.

probe microanalysis measurements in different positions at the interface (Table 1), suggested the identification of the intermetallic phases. The brighter layer about 30 μm thick, marked by A, richer in iron and closer to the steel substrate, is characterized by a composition which is in the stability range of orthorhombic Fe_2Al_5 phase. It shows the serrated tongue-like shape typical of Fe_2Al_5 phase formed in dipping experiments between pure iron and pure aluminium [6-8, 25]. The darker and thinner layer (about 17 μm), labelled B, closer to the aluminium foam, could be identified as the minor phase $FeAl_3$ formed between solid iron and molten aluminium. The aluminium side of this layer shows a blocky structure, characterised by darker regions within it with texture and shade similar to that of Al alloy that could be ascribed to aluminium that remains liquid during the formation of the intermetallic phase. The interface of AlSi10 specimen highlights the formation of three intermetallic layers about 8 μm thick each. While A and B layers are quite continuous the C one appears interrupted. The SEM-EDX results indicate a strong influence of silicon in the formation of the intermetallic phases between foam and low carbon steel substrate.

Moving from aluminium foam to the substrate: a β-$Al_{4.5}FeSi$ phase (marked by C), also known as τ_6, followed by an α-Al_8Fe_2Si phase (marked by B), also known as τ_5, typical of rich Al corner in the AlFeSi phase diagram can be identified, while a $Fe_2(Al,Si)_5$ phase, characterised by a composition similar to that of Fe_2Al_5 intermetallic layer, observed for AlMg1Si0.6 precursor, can be observed close to iron (marked by A).

To evaluate the mechanical properties of the constituent phases, nano hardness tests were performed across the interface intermetallic layer. Fig. 5 shows some random areas of AlMg1Si0.6 and AlSi10 samples in which indentations have been performed. Secondary and back scattered electron images of each area are presented together in order to better recognise to which layer one indentation belongs. The mean Vickers hardness values and the sample standard deviations are reported in Table 2 for each layer. Statistical analysis of variance (ANOVA) of the results supported by the multiple comparison Tuckey test allowed to distinguish two layers for AlMg1Si0.6 and three layers of different hardness for AlSi10 precursor. Two and three phases of increasing

Table 1 Elemental composition (wt%) in positions indicated by capital letters in Fig. 4. The top part refers to AlMg1Si0.6, the bottom part to the AlSi10 starting precursor.

AlMg1Si0.6	O	Al	Si	Mn	Fe
A	1.59	54.23	0.89	0.57	42.72
B	1.79	59.36	0.63	0.40	37.81
AlSi10	O	Al	Si	Mn	Fe
A	1.58	51.52	3.40	0.49	43.01
B	2.05	54.44	11.16	0.42	31.93
C	1.94	55.19	15.91	0.09	26.87

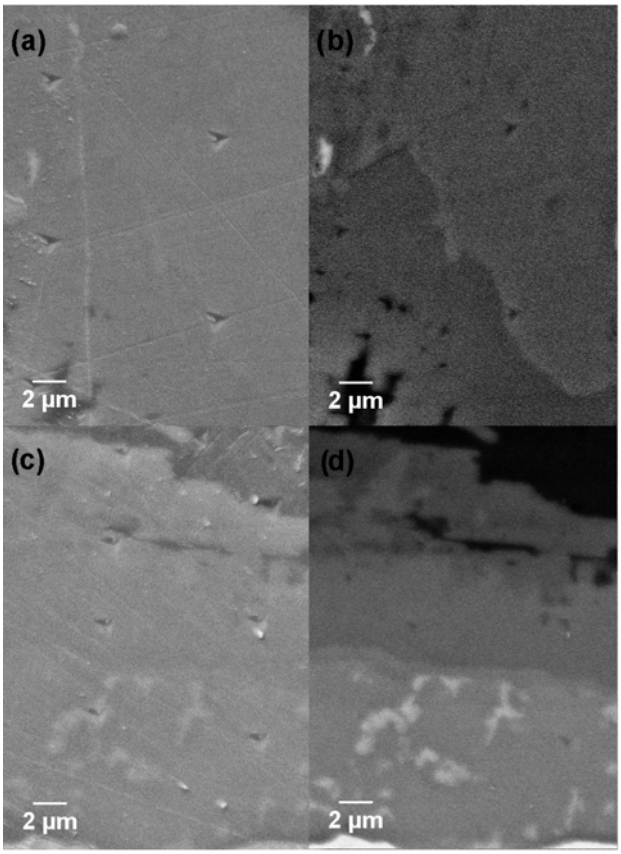

Fig. 5 Scanning electron micrographs of the foam/steel interface showing the nano indentation spots: (a) and (b) SE and BSE signal respectively for AlMg1Si0.6 alloy; (c) and (d) SE and BSE signal respectively for AlSi10 alloy.

hardness can be distinguished going from foam to steel substrate for AlMg1Si0.6 and AlSi10 precursors respectively. These results suggest the importance of elemental diffusion from the molten aluminium matrix (foam) in the steel substrate.

3.3 Microstructure Characterization of Specimens' Surface

X-ray diffraction measurements and SEM observations were performed on the surface of the specimen after removal of foam and intermetallic material by subsequent grinding steps. Figs. 6 and 7 report X-ray diffraction patterns of specimens foamed starting from AlSi10 and AlMg1Si0.6 precursors respectively. Fig. 6a shows that typical reflections of Al and Si were found in the uppermost layer of the sample, while after further polishing, typical reflections of Fe_2Al_8Si (phase α) and $FeAl_5Si$ (phase β) could be detected (Figs. 6b-6d). The simultaneous presence of different phases in the two samples is due to the irregular shape of the intermetallic layers as it is evident from Fig. 4. Finally, when XRD were collected on the deepest layer (Fig. 6e), no more Al and Si were detected and only phases α and β were found.

Fig. 7a-7d show the diffractogram of samples prepared starting from AlMgSi0.6 precursor. In the uppermost layers (Figs. 7a and 7b), reflections of Al and $FeAl_3$ were found. Instead, after further polishing (Figs. 7c and 7d), no more Al was detected and typical reflections of Fe_2Al_5, along with the ones of $FeAl_3$, were found. A very strong reflection at about 2θ = 42.6° was detected and it was attributed to the elongation along the c-axis of Fe_2Al_5 phase [6]. Table 3 reports the phases and the relative abundances detected in the samples analyzed.

Scanning electron micrographs (BEI) of representative portions of the surface of AlSi10 specimen after subsequent removal of material underline the presence of the different intermetallic phases as soon as the bonding layer is penetrated. In Fig. 8, at small magnification, a predominant dark grey contribution ascribed to the still present foam is evident together with brighter areas related to intermetallic phases.

Higher magnification observations show that the brighter contribution seems to be due to two different phases of different composition. On the basis of the elemental weight percentages reported in Table 4 the brighter area, with higher Fe concentration, can be ascribed to α-Al8Fe2Si phase (highlighted by letter B) while the less bright area, characterised by less iron, is related to β-Al4.5FeSi phase (underlined by letter C). The contribution of α-Al8Fe2Si phase increases as the progressive removal of material go on in agreement with cross section SEM observations. Further removal of intermetallic shows the contribution of a third

Table 2 Vicker's hardness values and standard deviation for indentations in intermetallic layer of different composition at the interface between foam and steel substrate: the top refers AlMg1Si0.6; the bottom to the AlSi10 starting precursor.

AlMg1Si0.6	HV	Sample std. dev	Number of Indentations
A	1050.87	70.15	9
B	893.55	63.77	5
AlSi10	**HV**	**Sample std. dev**	**Number of Indentations**
A	1142.02	72.91	12
B	1003.35	45.16	10
C	830.00	61.23	8

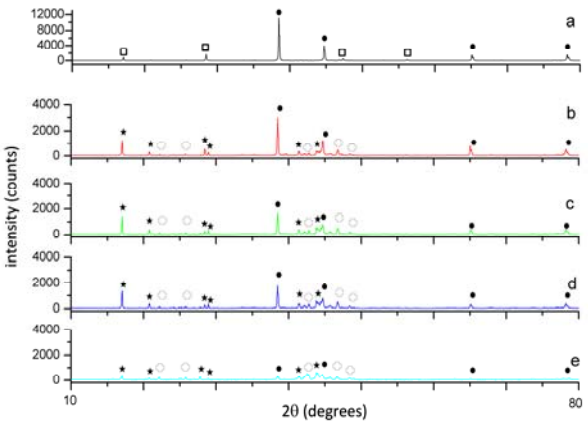

Fig. 6 XRD patterns of the intermetallic layer surface starting from AlSi10 precursor. Diffractograms from a toward *e* are representative of increasing removal of material, that is further penetration in the steel substrate. Different symbols highlight the various phases detected: Al •, Si □, α-Al_8Fe_2Si ◌, β-$Al_{4.5}FeSi$ ☆.

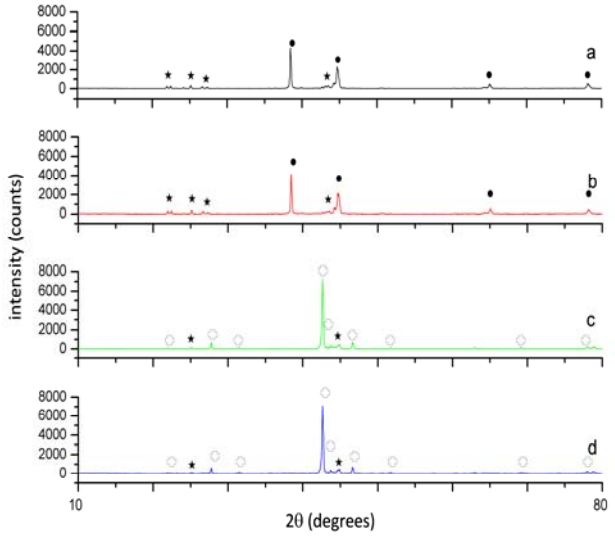

Fig. 7 XRD patterns of the surface of the intermetallic layer started from AlMg1Si0.6 precursor. Diffractograms from *a* toward *e* are representative of increasing removal of material, that is further penetration in the steel substrate. Different symbols highlight the various phases detected: Al •, Fe_2Al_5 ✧ , $FeAl_3$ ☆.

Table 3 Phases and relative abundance detected after subsequent grinding steps (XX: large amount, X: medium amount, XO: low amount, O: traces). The top part refers to AlSi10; the bottom part refers to the AlMg1Si0.6 starting precursor.

AlSi10	Al	Si	Fe_2Al_8Si (α)	$FeAl_5Si$ (β)
a	XX	XX	O	O
b	X	X	X	X
c	XO	XO	X	X
d	XO	XO	X	X
e	O	-	X	X
AlMg1Si0.6	Al		$FeAl_3$	Fe_2Al_5
a	XX		X	-
b	XX		X	-
c	-		X	XX
d	-		X	XX

phase (highlighted by letter A) with higher iron content (~43 wt%) in agreement with existence of $Fe_2(Al,Si)_5$ phase near the steel substrate. The elemental composition of these areas correspond to those detected across the specimen cross section at positions indicated by letters B, C and A, respectively which confirms the formation of an intermetallic layer in the steel substrate when the liquid foam comes in contact with the solid substrate.

Similarly the progressive removal of material from the surface of AlMg1Si0.6 specimen underlines the increase of the contribution due to the Fe_2Al_5 phase, richer in iron, (regions identified by A in right column of Fig. 9) that forms at the steel substrate respect to $FeAl_3$ (highlighted by B in right column of Fig. 9) in agreement with SEM observations on the cross section in Fig. 4. The elemental compositions are presented in Table 4.

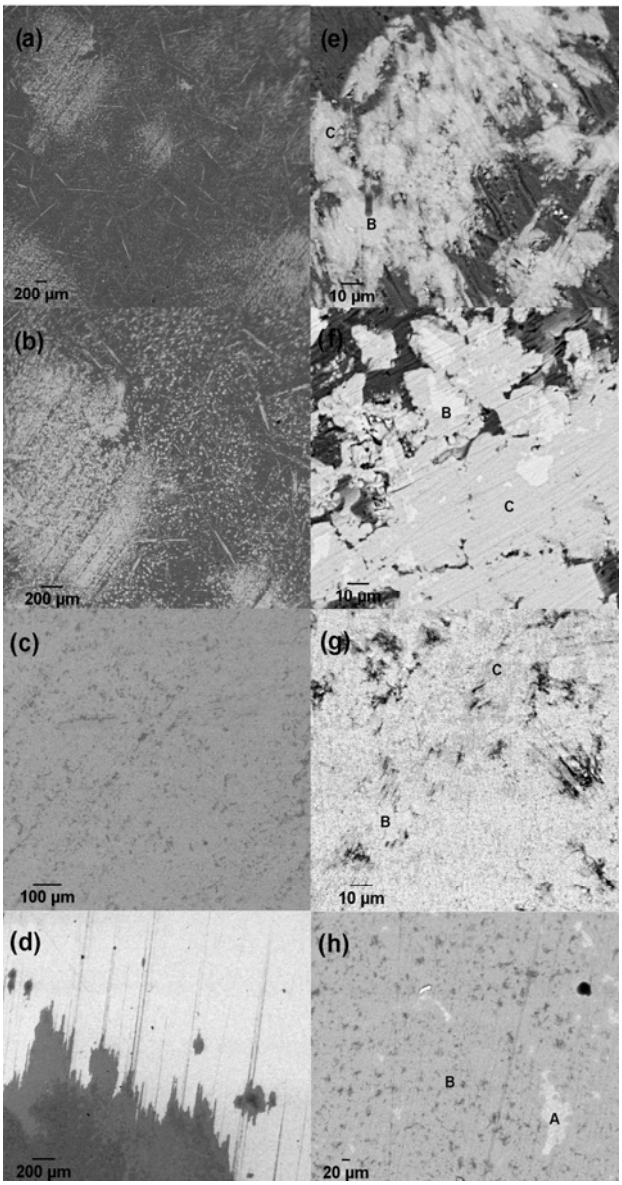

Fig. 8 Scanning electron micrographs (BSE signal) at low magnification (panels a, b, c, d) and at high magnification (paniels e, f, g, h) of the surface of AlSi10 specimen foamed in argon. Going from top to bottom is representative of gradual penetration in the steel substrate.

Table 4 Elemental composition (wt%) in positions indicated by capital letters in Fig. 8 (upper part) and in Fig. 9 (bottom part).

AlSi10	Al	Si	Mn	Fe
a_ B	56.83	11.33	0.58	31.27
a_ C	56.35	15.85	0.47	27.32
b_ B	56.14	10.75	0.42	32.70
b_ C	56.54	15.98	0.31	27.17
c_B	57.65	11.01		31.34
c_C	56.59	16.38		27.02
d_A	51.68	4.65	0.65	43.02
d_B	57.49	12.24	0.39	29.88
AlMg1Si0.6	Al	Si	Mn	Fe
a_B	60.59	0.55	0.10	38.76
b_A	55.58	0.76	0.57	43.10
b_B	60.35	0.50	0.43	38.72
c_A	56.03	0.65	0.59	42.73
c_B	60.61	0.41	0.58	38.40

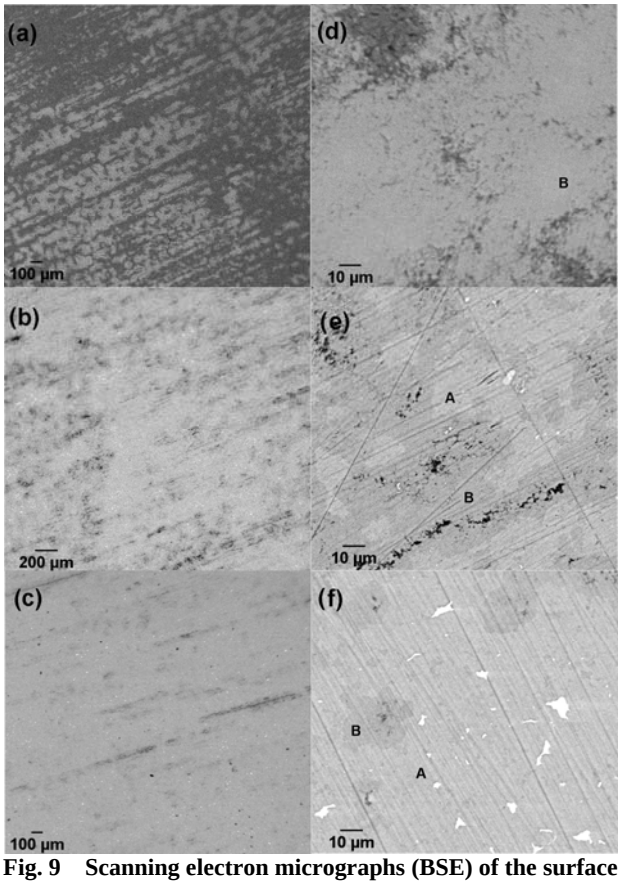

Fig. 9 Scanning electron micrographs (BSE) of the surface of AlMg1Si0.6 specimen foamed in argon at low magnification (panels a, b, c) and high magnification (panels d, e, f). Going from top to bottom is representative of gradual penetration in the steel substrate.

4. Conclusions

A detailed microstructural characterisation of the intermetallic layer at the foam/substrate interface showed a uniform and continuous layer formed when the foaming process was performed in argon flux, even for silicon rich precursor. A double layer is observed for low silicon precursor showing the presence of Fe_2Al_5 near steel and $FeAl_3$ close to Al foam. A three phase layer characterises the intermetallic layer formed by the precursor with high Si percentage. Going from the foam to the substrate: β ($FeAl_5Si$), α (Fe_2Al_8Si) and $Fe_2(Al,Si)_5$ can be identified. Though the major elements found in the intermetallic layers are the same, i.e. Al, Fe and Si, the morphological and mechanical properties of the phases formed are the result of the different percentages of these elements, underlying the importance of elemental interdiffusion in the process of bonding between foam and substrate. The results provide some contribution to the knowledge of the interactions between Al foams of different composition (molten at the foaming temperature) and solid steel. Further analysis considering different process parameters (temperature, time, atmosphere and cooling conditions) is in progress. It is supposed to yield better information on the mechanisms of diffusion of elements and on the growth kinetics of the intermetallic phases which strongly influences the thickness of the interface layer. Furthermore, a mechanical characterization of the joint will be studied (peel test and/or shear test) in order to compare the mechanical performances of the different types of intermetallic with different thickness and hardness.

Acknowledgments

The research has been carried out in the frame of the INTEMA research project funded by the Italian Ministry of Research under the “PRIN” programme and the Tecnopole Programme founded by the Administration of Emilia Romagna Region.

References

[1] L. Bonaccorsi, N. Proverbio, N. Raffaele, Effect of interface bonding on the mechanical response of aluminum foam reinforced steel tubes, Journal of Materials Science 45 (2010) 1514-1522.

[2] L. Vendra, A. Rabiei, A study on aluminum-steel composite metal foam processed by casting, Materials Science and Engineering A 465 (2007) 59-67.

[3] R. Neugebauer, C. Lies, J. Hohlfeld, T. Hipke, Adhesion in sandwiches with aluminum foam core, Production Engineering, Research and Development 1 (2007) 271-278.

[4] M. Monno, V. Mussi, D. Negri, Aluminum foam/steel inteface formed during foaming process in air or argon flow: a microstructural comparison, in: Cellular Materials-CELLMAT, 2010, pp. 313-319.

[5] M. Monno, V. Mussi, D. Negri, A. Rota, S. Valeri, On the influence of some proces parameters on aluminum foam/steel substrate bonding, in: 7th International Conference on Porous Metals and Metallic Foams, METFOAM, 2011, pp. 569-574.

[6] H.R. Shaverdi, M.R. Ghomashchi, S. Shabestari, J. Hejazi, Microstructural analysis of interfacial reaction between molten aluminium and solid iron, Journal of Matererials Science 36 (2002) 1061-1066.

[7] K. Bouchè, F. Barbier, A. Coulet, Intermetallic compound layer between solid iron and molten aluminum, Materials Science Engineering A 249 (1998) 167-165.

[8] A. Bouayad, Ch. Gerometta, A. Bekebir, A. Ambari, Kinetic interactions between solid iron and molten aluminum, Materials Science Engineering A 363 (2003) 53-61.

[9] V.I. Dybkov, Reaction diffusion in heterogeneous binary systems (part 1), Journal of Materials Science 21 (1986) 3085-3090.

[10] V.I. Dybkov, Reaction diffusion in heterogeneous binary systems (part 2), Journal of Materials Science 21 (1986) 3078-3084.

[11] S.H. Hwang, J.H. Song, Y.S. Kim, Effect of carbon content of carbon steel on its dissolution into a molten aluminium alloy, Materials Science Engineeriang A (390) (2005) 437-443.

[12] T. Sasaki, T. Yakou, K. Mochiduki, K. Ichinose, Effects of carbon contents in steels on alloy layer growth during hot dip aluminium coating, ISIJ International 45 (2005) 1887-1892.

[13] K.A. Nazari, S.G. Shabestari, Effect of micro alloying elements on the interfacial reactions between molten aluminum and tool steel, Journal of Alloys and Compounds 478 (2009) 523-530.

[14] S.G. Shabestari, The effect of iron and manganese on the formation of intermetallic compounds in aluminum-silicon alloys, Materials Science and Engineering A 383 (2009) 289-298.

[15] H. Springer, A. Kostka, E.J. Payton, D. Raabe, A. Kaysser-Pyzzalla, G. Eggeler, On the formation and growth of intermetallic phases during interdiffusion between low-carbon steel and aluminum alloys, Acta Materialia 59 (2011) 1586-1600.

[16] Y. Tanaka, M. Kajihara, Morphology of compounds formed by isothermal reactive diffusion between solid Fe and liquid Al, Materials Transactions 50 (2009) 2212-2220.

[17] J. Sacha, Seeded Region Growing Tool, IJ-Plugins Project, ij-plugins_toolkit v.1.6.0, http://ij-plugins.sourceforge.net/plugins/segmentation/srg.html (accessed Apr. 4, 2011).

[18] W.S. Rasband, ImageJ, U. S. National Institutes of Health, Bethesda, Maryland, USA, (1997-2005).

[19] F. Aguet, D. van de Ville, M. Unser, Model-based 2.5-D deconvolution for extended depth-of-field in brightfield microscopy, IEEE Trans. Image Process 17 (2008) 1144-1153.

[20] R. Adams, L. Bischof, Seeded region growing, IEEE Trans on Pattern Analysis and Machine Intelligence 16 (1994).

[21] W.C. Oliver, G.M. Pharr, An improved technique for determining hardness and elastic modulus using load and displacement sensing indentation experiments, Journal of Materials Research 7 (1992) 1564-1583.

[22] H. Glasbrenner, E. Nold, Z. Boss, The influence of alloying elements on the hot-dip aluminizing process and on the subsequent high-temperature oxidation, Journal of Nuclear Materials 249 (1997) 39-45.

[23] W. Fragner, B. Zberg, R. Sonnleitner, P. Uggowitzer, J. Loffler, Interface reactions of Al and binary Al alloys on mild substrates in controlled atmpsphere, Materials Science Forum 519-521 (2006) 1157-1162.

[24] M.V. Akdeniz, A.O. Mekhrabov, The effect of substitutional impurities on the evolution of Fe-Al diffusion layer, Acta Materialia 46 (1998) 1185-1198.

[25] G.H. Awan, F. ul Hasan, The morphology of coating/substrate in hot-dip-aluminized steels, Materials Science Engineering A 472 (2008) 157-165.